



Cite this: *Phys. Chem. Chem. Phys.*,
2015, 17, 17391

Utilizing alkoxyphenyl substituents for side-chain engineering of efficient benzo[1,2-*b*:4,5-*b'*]-dithiophene-based small molecule organic solar cells†

Zhengkun Du,^{ab} Weichao Chen,^a Meng Qiu,^a Yanhua Chen,^{ac} Ning Wang,^a
Ting Wang,^a Mingliang Sun,^{*c} Donghong Yu^{*bd} and Renqiang Yang^{*a}

A new two-dimensional (2D) conjugated small molecule, namely DCA3TBDTP, with an alkoxyphenyl substituted benzo[1,2-*b*:4,5-*b'*]dithiophene (BDT) unit as the central core, octyl cyanoacetate as the end-capped groups and terthiophene as the π -linked bridge, was designed and synthesized for solution-processed organic solar cells (OSCs) as an electron donor material, in which an alkoxyphenyl group was introduced as a weak electron-donating side chain of the BDT moiety. The DCA3TBDTP molecule exhibited good solubility, a deep highest occupied molecular orbital (HOMO) level (−5.25 eV), an appropriate optical band-gap (1.82 eV) and a high decomposition temperature (362 °C). By applying the simple solution spin-coating fabrication process, the bulk heterojunction (BHJ) OSCs based on DCA3TBDTP and [6,6]-phenyl-C₆₁-butyric acid methyl ester (PC₆₁BM) exhibited a good power conversion efficiency (PCE) of 4.51% with a high open-circuit voltage (V_{oc}) of 0.90 V when thermal annealing at only 70 °C.

Received 6th May 2015,
Accepted 1st June 2015

DOI: 10.1039/c5cp02632f

www.rsc.org/pccp

Introduction

As described in a report from Chen *et al.* in 2011,¹ benzo[1,2-*b*:4,5-*b'*]dithiophene (BDT, as the core) based acceptor–donor–acceptor (A–D–A) small molecule organic solar cells (SMOSC) reached their power conversion efficiency (PCE) of 5.44%, which was mainly attributed to BDT's large and rigid planar structure as a structural analogue of the electron-rich anthracene moiety with enhanced electron delocalization and promoted cofacial π – π stacking in the solid state, thus being favored for charge transport in OSC devices.^{2–5} This had made it a very good electron-donating unit in high-performance conjugated donor materials in SMOSCs with their promisingly comparable PCEs (exceeding 9%) to their polymer counterparts,^{6–8} possessing great advantages of relatively simple synthesis and purification and well-defined structures thus, less batch-to-batch variation, possible versatile structural design

thus, easier control of energy levels, and high charge carrier mobilities.^{9,10} Since then, significant progress on such BDT based SMOSCs has been achieved by incorporating a series of dye building blocks as various acceptor motifs such as 3-ethylrodanine,¹¹ indenedione (1,3-indandione),¹² 1,3-dimethylbarbituric acid,⁹ and DPP,¹³ as well as by symmetrical π -conjugated substitutions on the phenyl unit of BDT with alkylthienyl,¹⁴ alkylphenyl,¹⁵ alkylsilyl ethynyl¹⁶ and alkylselenophene¹⁷ groups. Such π -conjugated substituents in the orthogonal direction of BDT result in 2-dimensional (2D) expanded delocalization of π -electrons to the conjugated side groups thus, better interchain π – π stacking, which could benefit the exciton diffusion and charge transport (in comparison to 1D BDT units substituted with non-conjugated side groups like dialkoxy¹¹ or dialkylthiol⁶ substituents), therefore allowing improved broad light absorbance and deep highest occupied molecular orbital (HOMO) energy levels which could contribute to a relatively high open-circuit voltage (V_{oc}) (ca. 0.90–1.0 V) and high efficiency (PCE > 7%).^{6,18}

State-of-the-art methods involving altering the side chain structures on the BDT moiety have presented the great ability to fine tune electronic properties such as energy levels, bandgap, and charge carrier mobility, *etc.*^{6,18} Among the vast variety of developed BDT-based electron-donating derivatives, systematic investigations on 1D alkyl-, alkoxy-, and alkylthiol-BDT based SMOSCs have been carried out by Chen *et al.* in a series of papers: the choice of the weaker electron-donating ability of alkylthiol- than alkoxy-BDT based SMOSCs with a V_{oc} of 0.91 V;⁶

^a CAS Key Laboratory of Bio-based Materials, Qingdao Institute of Bioenergy and Bioprocess Technology, Chinese Academy of Sciences, Qingdao 266101, China. E-mail: yangrq@qibebt.ac.cn; Fax: +86-532-80662778; Tel: +86-532-80662700

^b Department of Chemistry and Bioscience, Aalborg University, DK-9220, Aalborg, Denmark. E-mail: yu@bio.aau.dk

^c Institute of Materials Science and Engineering, Ocean University of China, Qingdao 266100, China. E-mail: mlsun@ouc.edu.cn

^d Sino-Danish Centre for Education and Research (SDC), Niels Jensens Vej 2, DK-8000, Aarhus, Denmark

† Electronic supplementary information (ESI) available. See DOI: 10.1039/c5cp02632f

the replacement of a strong electron donating 2-ethylhexyloxy side chain on the BDT unit with a less electron-donating octyl side chain resulting in an even lower HOMO energy level (-5.02 eV) and thus a much higher V_{oc} (0.98 V).¹⁹ However, for 2D π -conjugated units attached to BDT in SMOSCs, only strong electron donors like alkylthiophene, alkylbenzene, alkylselenophene, and alkylsilylthyne^{14–17} have been reported. In order to systematically engineer such side chain dependency, the promising, less strong alkoxyphenyl substituents ought to be taken into consideration for the molecular design. An alkoxyphenyl side group has been recently been used in 2D BDT based polymers by both Zou's group, with PBDTPO-DTBO,²⁰ and our group, with PBDTPF-DTBT²¹ (with fluorinated alkoxyphenyl side chain), which demonstrated high PCEs of 6.2% and 7.02%, and mobilities of up to 0.22 and 0.034 cm^2 (V s)⁻¹, respectively. Meanwhile, we designed and synthesized a new small molecule, BDT-PO-DPP, by replacing the alkoxy groups in the BDT unit with alkoxyphenyl ones for extended conjugation along the side chain directions; this gave a PCE of 5.63% after thermal annealing at 110 °C.²² In order to systematically explore the molecular structure dependency on electronic properties like energy level and charge mobility, further design of more SMOSCs based on alkoxyphenyl substituted BDT would be fundamentally essential. On the other hand, being one of the widely used end-capped blocks for building high-performance SMOSCs due to its simple conjugated structure and strong electron-withdrawing ability, octyl cyanoacetate could not only effectively regulate the energy levels of the HOMO and lowest unoccupied molecular orbital (LUMO), but also greatly improve the solubility of the targeted small molecules.^{1,9,11–13,18}

Considering the above discussion, in this work, for the side-chain engineering of BDT based high PCE SMOSCs, we introduced the weak electron-donating group *para*-alkoxyphenyl as an aromatic substituent on BDT to obtain a new 2D conjugated small molecule DCA3TBDTP (Scheme 1). This compound consists of three segments: octyl cyanoacetate as the end-capped groups, terthiophene as the π -linked bridge and alkoxyphenyl substituted BDT as the central core. The molecule DCA3TBDTP exhibited excellent solubility in common organic solvents and good thermal stability, and the DCA3TBDTP-PC₆₁BM blend film showed a hole mobility of up to 2.74×10^{-4} cm^2 (V s)⁻¹, which was measured *via* the space-charge limit current (SCLC) model. BHJ-OSCs fabricated with DCA3TBDTP as the donor and PC₆₁BM as the acceptor showed a good PCE of 4.51% with

a high open-circuit voltage of 0.90 V after thermal annealing at a low temperature (70 °C).

Experimental section

Materials

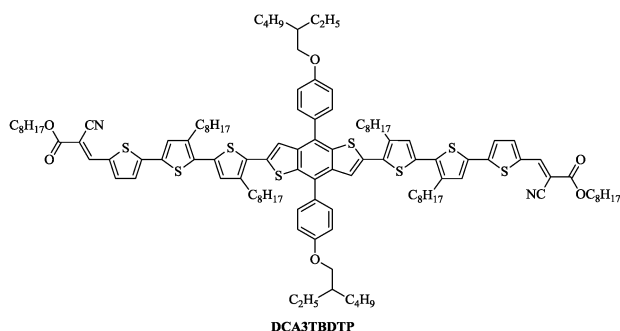
All chemicals, unless otherwise specified, were purchased from commercial sources and used as received. Toluene and tetrahydrofuran (THF) were freshly distilled in the presence of sodium and benzophenone under a nitrogen atmosphere prior to use. 5''-Bromo-4',4''-dioctyl-2,2':5',2''-trithiophene-5-carbaldehyde (**6**) was synthesized as reported in the literature.²³

Instruments and measurements

Nuclear magnetic resonance (NMR) spectra were measured on a Bruker AVANCE-III 600 spectrometer. High resolution mass spectra (HRMS) were recorded under the APCI mode on a Bruker Maxis UHRTOF spectrometer. Thermal gravimetric analysis (TGA) measurements were performed on an STA-409 at a heating rate of 10 °C min^{-1} . Differential scanning calorimetry (DSC) analysis was carried out on a Perkin Elmer diamond differential scanning calorimeter. UV-vis absorption spectra were recorded with a Perkin Elmer Lambda 25 spectrophotometer. Cyclic voltammetry (CV) was performed using a CHI660D electrochemical workstation with a glassy carbon working electrode, a saturated calomel reference electrode (SCE), and a platinum wire counter electrode at a scan rate of 50 mV s^{-1} . Tetrabutylammonium phosphorus hexafluoride (Bu₄NPF₆, 0.1 M) in acetonitrile was used as the supporting electrolyte. The surface roughness and morphology of the thin films of the active layers were characterized using atomic force microscopy (AFM) on an Agilent 5400 working at the tapping mode. X-ray diffraction (XRD) patterns were recorded on a Bruker D8 Advance.

Fabrication and characterization of the organic solar cells

Photovoltaic devices were fabricated on pre-patterned indium tin oxide (ITO) coated glass substrates with the device geometry of ITO/PEDOT:PSS/DCA3TBDTP:PC₆₁BM/Ca(10 nm)/Al(100 nm). The ITO glass substrates were cleaned ultrasonically in acetone, toluene, methanol and isopropyl alcohol, sequentially. Then, oxygen plasma treatment was carried out for 20 min, then the substrates were spin-coated with PEDOT:PSS at 4000 rpm, and dried under an argon atmosphere for 30 min at 160 °C. The photosensitive layer was prepared by spin-coating a blend solution of the DCA3TBDTP and PC₆₁BM with a weight ratio of $3:1$, $2:1$ and $1:1$ in deoxygenated anhydrous chloroform on the ITO/PEDOT:PSS substrate in a glove box. The thickness of the active layer films was measured by a Dektak 150 profilometer was determined to be around 100 nm. Finally, Ca (10 nm) and aluminum (100 nm) were thermally evaporated and deposited on the top of the active layer in a defined area of 0.1 cm^2 at a vacuum pressure of $\sim 2 \times 10^{-4}$ Pa. The current density-voltage (J - V) characteristics were recorded with a Keithley 2420 source measurement under AM 1.5G illumination (100 mW cm^{-2}) from a Newport solar simulator. A standard silicon solar cell was used



Scheme 1 Chemical structure of DCA3TBDTP.

to calibrate the light intensity. The external quantum efficiencies (EQE) of the OSCs were measured using a certified Newport incident photon conversion efficiency (IPCE) measurement system.

Synthesis

The synthetic route of the targeted small molecule is presented in Scheme 2.

1-Bromo-4-(2'-ethylhexyloxy)benzene (2). Under an argon atmosphere, 4-bromophenol (5.20 g, 30 mmol) and K_2CO_3 (4.98 g, 36 mmol) were added into 100 mL of DMF in a two-neck flask. After stirring for 5 min, 2-ethylhexyl bromide (6.75 g, 35 mmol) was added *via* a syringe. The mixture was heated to 120 °C for 24 h in darkness. The cooled mixture was poured into water and then extracted with diethyl ether three times. The combined organic phase was dried over anhydrous magnesium sulfate ($MgSO_4$). After removing the organic solvents, the residue was purified on a silica gel column eluting with petroleum ether. Compound 2 was obtained as a pale yellow oil (7.53 g, 90% yield). 1H NMR (600 MHz, $CDCl_3$): δ (ppm): 7.36 (d, 2H), 6.78 (d, 2H), 3.80 (d, 2H), 1.70 (m, 1H), 1.51–1.28 (m, 8H), 0.93–0.89 (m, 6H). ^{13}C NMR (150 MHz, $CDCl_3$): δ (ppm): 158.52, 132.15, 116.34, 112.46, 70.78, 39.32, 30.49, 29.06, 23.83, 23.04, 14.08, 11.09.

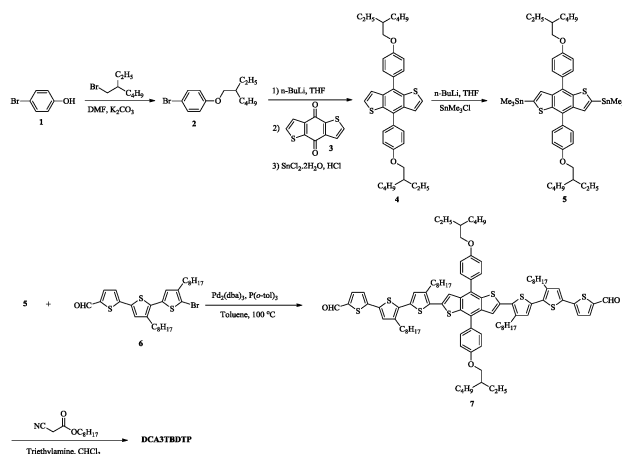
4,8-Bis(4-ethylhexyloxy-1-phenyl)-benzo[1,2-*b*:4,5-*b'*]dithiophene (4). In a 200 mL argon purged three-neck flask, *n*-BuLi (15 mL, 1.6 M in hexane) was added dropwise into a solution of 2 (6.85 g, 24 mmol) in THF (50 mL) at –78 °C. The mixture was kept at –78 °C for 1.5 h. Subsequently, benzo[1,2-*b*:4,5-*b'*]dithiophene-4,8-dione (1.76 g, 8 mmol) was added quickly, and the mixture was stirred for 3 h at 55 °C. After cooling to room temperature, a solution of $SnCl_2 \cdot 2H_2O$ (14.45 g, 64 mmol) in 10% HCl (25.6 mL) was added and then the mixture was stirred for an additional 2.5 h at 55 °C. The mixture was quenched with 60 mL of deionized water and then extracted with diethyl ether. The combined organic extract was dried with anhydrous $MgSO_4$ and the solvent was evaporated under vacuum. The residue was purified *via* a silica gel column using petroleum ether as the eluent to obtain compound 4 as a white solid (1.82 g, 38% yield). 1H NMR (600 MHz, $CDCl_3$): δ (ppm): 7.62 (d, 4H), 7.38 (d, 2H), 7.34 (d, 2H), 7.09 (d, 4H),

3.96 (d, 4H), 1.80 (m, 2H), 1.60–1.36 (br, 16H), 0.98 (t, 6H), 0.94 (t, 6H). ^{13}C NMR (150 MHz, $CDCl_3$): δ (ppm): 159.25, 138.30, 136.24, 131.41, 130.50, 130.01, 126.99, 123.09, 114.74, 70.57, 39.49, 30.61, 29.15, 23.94, 23.10, 14.13, 11.19.

2,6-Bis(trimethyltin)-4,8-bis(4-ethylhexyloxy-1-phenyl)-benzo[1,2-*b*:4,5-*b'*]dithiophene (5). In a 100 mL argon purged flask, *n*-BuLi (3.25 mL, 1.6 M in hexane) was added into a dry THF solution (45 mL) of compound 4 (1.20 g, 2 mmol) at 0 °C. After the addition, the mixture was kept at room temperature for 1.5 h, and then $SnMe_3Cl$ (5.75 mL, 1.0 M in hexane) was added quickly *via* a syringe at 0 °C. The mixture was stirred overnight at room temperature. Subsequently, the mixture was poured into deionized water (40 mL) and extracted with diethyl ether three times. The combined organic phase was dried over anhydrous $MgSO_4$. After removing the organic solvents, the residue was recrystallized from acetone to afford the yellow solid compound 5 (1.10 g, 60% yield). 1H NMR (600 MHz, $CDCl_3$): δ (ppm): 7.64 (d, 4H), 7.38 (s, 2H), 7.10 (d, 4H), 3.97 (d, 4H), 1.80 (m, 2H), 1.60–1.36 (br, 16H), 0.99 (t, 6H), 0.94 (t, 6H), 0.35 (t, 18H). ^{13}C NMR (150 MHz, $CDCl_3$): δ (ppm): 159.05, 142.59, 141.62, 137.07, 132.06, 130.86, 130.57, 128.45, 114.64, 70.49, 39.54, 30.63, 29.17, 23.96, 23.11, 14.14, 11.22, –8.36.

Synthesis of compound (7). In a 100 mL flame-dried flask, compound 6 (0.76 g, 1.32 mmol) and 5 (0.55 g, 0.6 mmol) were dissolved in anhydrous toluene (25 mL). After the solution was degassed with argon three times, $Pd_2(dba)_3$ (16 mg, 0.018 mmol) and $P(o-tol)_3$ (32 mg, 0.108 mmol) were added under argon protection quickly. The reaction mixture was slowly heated to 100 °C for 36 h under an argon atmosphere. The cooled mixture was poured into deionized water and extracted with $CHCl_3$ three times. The combined organic phase was dried over anhydrous $MgSO_4$ and concentrated under vacuum. The crude residue was purified *via* a silica gel column using petroleum/ CH_2Cl_2 (v/v, from 1 : 1 to 1 : 5) as the eluent to obtain compound 7 (0.64 g, 67% yield) as a red solid. 1H NMR (600 MHz, $CDCl_3$): δ (ppm): 9.85 (s, 2H), 7.68 (d, 4H), 7.66 (d, 2H), 7.36 (s, 2H), 7.21 (d, 2H), 7.18 (s, 2H), 7.11 (d, 4H), 7.00 (s, 2H), 3.97 (d, 4H), 2.77 (m, 8H), 1.81 (m, 2H), 1.69–1.61 (m, 8H), 1.53–1.23 (m, 56H), 0.99 (t, 6H), 0.94 (t, 6H), 0.88–0.85 (m, 12H). ^{13}C NMR (150 MHz, $CDCl_3$): δ (ppm): 182.43, 159.40, 146.97, 141.52, 141.32, 140.93, 138.49, 137.42, 136.78, 136.25, 134.26, 133.41, 132.60, 131.68, 130.97, 130.41, 129.42, 129.35, 129.14, 123.98, 121.45, 114.86, 70.61, 39.52, 31.89, 31.85, 30.60, 30.37, 29.53, 29.51, 29.47, 29.41, 29.39, 29.29, 29.23, 29.17, 23.93, 23.10, 22.69, 22.66, 14.13, 14.11, 11.19.

Synthesis of DCA3TBDTP. Under an argon atmosphere, octyl cyanoacetate (0.55 g, 2.8 mmol) was added to a stirred chloroform solution (30 mL) of triethylamine (0.05 mL) and compound 7 (0.40 g, 0.25 mmol) *via* a syringe at 28 °C. The solution was stirred at 28 °C for 40 hours under an argon atmosphere, and was then added with water (35 mL) and extracted with $CHCl_3$ three times. The organic phase was dried over anhydrous $MgSO_4$ and the solvent was removed under vacuum. The crude product was purified by means of column chromatography over a silica gel using petroleum/ CH_2Cl_2 (v/v, 1 : 2) as the eluent and then recrystallized in a mixing solvent of methanol–chloroform to obtain DCA3TBDTP (0.35 g, 72% yield) as a black solid. 1H NMR (600 MHz, $CDCl_3$), as found in Fig. S3 (ESI†),



Scheme 2 Synthetic route for DCA3TBDTP.

δ (ppm): 8.25 (d, 2H), 7.68 (d, 4H), 7.64 (d, 2H), 7.37 (s, 2H), 7.23 (s, 2H), 7.20 (d, 2H), 7.12 (d, 4H), 7.01 (d, 2H), 4.29 (t, 4H), 3.97 (d, 4H), 2.77 (m, 8H), 1.81 (m, 2H), 1.75 (m, 4H), 1.70–1.61 (m, 8H), 1.53–1.23 (m, 76H), 0.99 (t, 6H), 0.94 (t, 6H), 0.90–0.85 (m, 18H). ^{13}C NMR (150 MHz, CDCl_3), δ (ppm): 163.11, 159.41, 147.32, 146.17, 141.36, 141.15, 139.33, 138.49, 136.79, 136.23, 134.23, 134.17, 133.09, 131.81, 130.96, 130.41, 129.59, 129.42, 129.41, 124.14, 121.48, 116.12, 114.86, 97.48, 70.61, 66.59, 39.52, 31.89, 31.85, 31.78, 30.60, 30.58, 30.37, 29.53, 29.48, 29.39, 29.29, 29.23, 29.19, 29.17, 29.16, 28.57, 25.81, 23.93, 23.10, 22.69, 22.65, 14.13, 14.12, 14.10, 11.19. MS (UHR-TOF): calcd. for $\text{C}_{118}\text{H}_{156}\text{N}_2\text{O}_6\text{S}_8$ $[\text{M}]^+$: 1952.9729; found: 1952.9724.

Results and discussion

Synthesis and characterization

The detailed synthetic route of the small molecule DCA3TBDTP is outlined in Scheme 2. Compound 5 and 6 were synthesized according to reported procedures.^{20,23} The important precursor 7 containing two aldehyde groups was synthesized by a Stille coupling reaction between compound 5 and 6. The target small molecule DCA3TBDTP was obtained by means of a Knoevenagel condensation between octyl cyanoacetate and the corresponding aldehyde, compound 7. The purity of the targeted compound for device fabrication was guaranteed by multiple column chromatographic purification and recrystallization in a mixing solvent of methanol–chloroform. The targeted compound was fully characterized using HRMS, ^1H and ^{13}C NMR (Fig. S3, ESI[†]). DCA3TBDTP shows good solubility in common organic solvents, which is a prerequisite for solution-processed SMOSCs.

Thermal stability

The thermal property of DCA3TBDTP was investigated through TGA and DSC. As shown in Fig. 1, DCA3TBDTP exhibited a good thermal stability with a decomposition temperature (T_d , 5% weight loss) at 362 °C under a nitrogen atmosphere, evidencing sufficient thermal stability for its device application. As shown in Fig. S1 (ESI[†]), the first thermal heating scan (heat 1 curve)

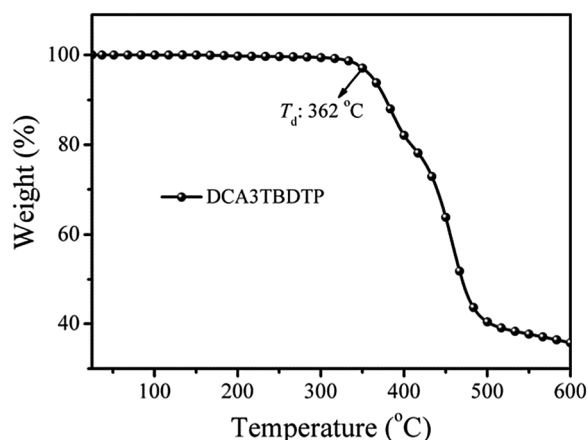


Fig. 1 TGA curve of DCA3TBDTP with a heating rate of 10 °C min^{−1} under a nitrogen atmosphere.

was applied in order to undo the thermal/solvent induced crystallization of the sample. Thermodynamic phase transition temperatures including the melting point and crystallization temperature were adopted from the second heating scan and cooling of the thermogram (heat 2 and cooling curve). Distinct melting peaks from both solvent induced (heat 1) and thermally crystallized (heat 2) samples reveal the formation of the crystal structure and therefore indicate the strong intermolecular interactions among the small molecules *via* π – π stacking within the aromatic moieties and hydrophobic interactions within the alkyl side chains. It is found that the main melting endotherm of DCA3TBDTP occurred at 192.84 °C and the corresponding melting enthalpy (ΔH_m) calculated from the integrated area of the melting peak was 39.96 J g^{−1}. During the cooling process, DCA3TBDTP showed a crystallization ΔH_m of 23.75 J g^{−1} at 180.87 °C, proving that the small molecule has an obvious tendency to crystallize,²⁴ while the larger enthalpy value of the solvent induced crystallization (ΔH_m of 44.80 J g^{−1}) indicates a higher degree of crystallinity than that of the materials crystallized *via* cooling, possibly indicating good phase separation between the donor DCA3TBDTP and the acceptor PC₆₁BM caused by solvent evaporation during spin-coating of the active layer materials.

Optical properties

Fig. 2 explored the normalized ultraviolet-visible (UV-vis) absorption of DCA3TBDTP in a dilute chloroform solution (5×10^{-6} mol L^{−1}) and in the thin film. The UV-vis absorption spectrum of DCA3TBDTP in solution exhibited an absorption peak at 500 nm with a maximum molar extinction coefficient (ϵ_{max}) of 8.68×10^4 L (mol cm)^{−1} (Fig. S2, ESI[†]), arising from intramolecular charge-transfer (ICT) between the donor and acceptor moieties. The shoulder peak ranging from 350–450 nm can be attributed to the π – π^* transitions of the conjugated units. The DCA3TBDTP thin film showed broader absorption across the visible region (300–700 nm) due to more effective electron push–pull effects and extended π – π packing of the molecular backbones in the solid state. Compared with that in solution, the thin film absorption peak displayed a bathochromic shift of about 73 nm, indicating the strong

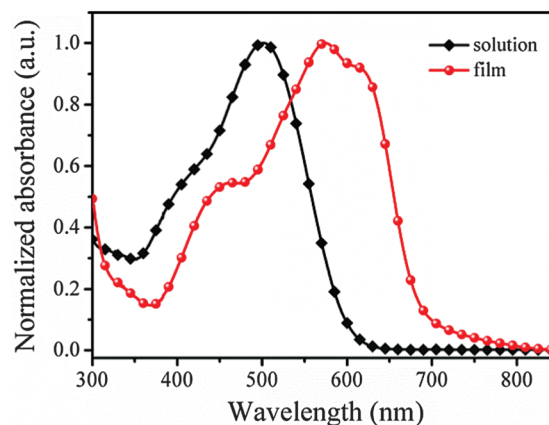


Fig. 2 Normalized UV-vis absorption spectra of DCA3TBDTP in a CHCl_3 solution and in a thin film.

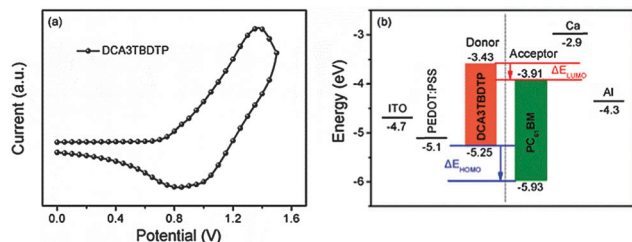


Fig. 3 (a) Cyclic voltammogram of DCA3TBDTP thin film at a scan rate of 50 mV s^{-1} . (b) Energy level diagrams of DCA3TBDTP and other materials used in SMOSCs.

intermolecular π - π interaction and aggregation in the solid state due to improved planar construction of the 2D side chains. The optical band gap ($\Delta E_{\text{g}}^{\text{opt}}$) of DCA3TBDTP is estimated to be 1.82 eV derived from the absorption onset of the thin film (683 nm). In terms of OSC design, such a low band gap of DCA3TBDTP will lead to a higher photocurrent, making this molecule more useful for OSC applications.

Electrochemical properties

The electrochemical properties of DCA3TBDTP were investigated using cyclic voltammetry (CV). A solution of tetrabutylammonium phosphorus hexafluoride (Bu_4NPF_6 , 0.1 M) in acetonitrile was used as the supporting electrolyte and the potential scan rate was 50 mV s^{-1} . As shown in Fig. 3a, DCA3TBDTP displayed one reversible oxidation wave. The redox potential of the Fc/Fc^+ internal reference is 0.39 V vs. SCE. The HOMO energy level of the target molecule was determined by the empirical formula of $E_{\text{HOMO}} = -e(E_{\text{Ox}} + 4.8 - E_{1/2}^+(\text{Fc}/\text{Fc}^+))$. The onset oxidation potential of DCA3TBDTP is 0.84 V, thus the corresponding HOMO energy level is -5.25 eV . Additionally, the LUMO energy level of DCA3TBDTP, calculated from the HOMO and optical band gap, is -3.43 eV .

The energy level diagrams of DCA3TBDTP and other materials used in the solution-processed BHJ SMOSCs are shown in Fig. 3b. The LUMO energy level offset (ΔE_{LUMO}) and HOMO energy level offset (ΔE_{HOMO}) of DCA3TBDTP/ PC_{61}BM are 0.48 eV and 0.68 eV, respectively. The relatively unmatched ΔE_{LUMO} and ΔE_{HOMO} values could lead to an unbalanced charge dissociation,²⁵ which is not conducive to the improvement of J_{sc} .

Geometry and electronic structure

Density functional theory (DFT) was employed to investigate the electronic structure of the molecule DCA3TBDTP with the B3LYP method at the 6-31G(d) basis set level in the gas phase (Fig. 4), and the DFT calculation was performed by the Gaussian 09 program.^{26–29} All the alkyl side chains were replaced with methyl groups to reduce the computational cost. The optimized molecular structure was confirmed to be in a stable local minimum of the ground state potential energy surface since there is no imaginary frequency by vibrational calculation at the same level of theory. The DFT-derived HOMO and LUMO energy levels of the molecule DCA3TBDTP were -5.10 eV and -2.91 eV , respectively. As shown in Fig. 4, DCA3TBDTP presented good planarity in the molecular

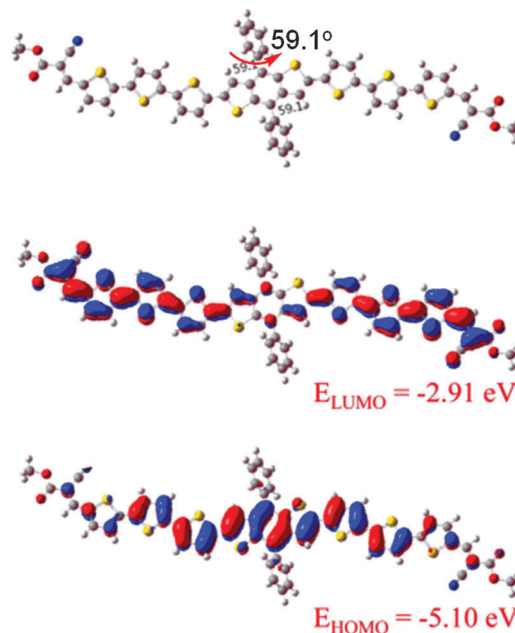


Fig. 4 Optimized molecular geometry and frontier molecular orbitals (isovalue surface 0.02 au) using DFT evaluated with the B3LYP method at the 6-31G(d) basis set level.

backbone direction. However, the pendant benzene rings on the benzodithiophene of DCA3TBDTP exhibited a torsion angle of about 59.1° because of the space steric effect, leading to a relatively poor planarity in the side chain direction.²²

Photovoltaic properties

BHJ photovoltaic devices were fabricated with a conventional architecture of ITO/PEDOT:PSS/DCA3TBDTP: PC_{61}BM /Ca/Al, and tested under simulated AM 1.5G illumination (100 mW cm^{-2}). Firstly, the blends of DCA3TBDTP and PC_{61}BM at different weight ratios were used to optimize the device performance. The detailed device parameters were summarized in Table 1. With an increase in the DCA3TBDTP/ PC_{61}BM blend ratio from 1:1 to 3:1, V_{oc} had no obvious change. However, the short circuit current density (J_{sc}) firstly increased from 5.40 mA cm^{-2} to 6.95 mA cm^{-2} and then decreased to 6.22 mA cm^{-2} . Compared with the V_{oc} and J_{sc} , the fill factor (FF) gradually increased. As is known to all, thermal annealing of the blend film could generally enhance the photovoltaic performance due to the improved

Table 1 Photovoltaic performance of SMOSCs based on DCA3TBDTP/ PC_{61}BM with different blend ratios, under AM 1.5G illumination (100 mW cm^{-2})

DCA3TBDTP/ PC_{61}BM (w:w)	Thermal annealing ^a	V_{oc} (V)	J_{sc} (mA cm^{-2})	FF (%)	PCE_{max} (PCE_{ave}) ^b (%)
1:1	No	0.89	5.40	42.40	2.04 (1.95)
2:1	No	0.89	6.95	61.88	3.83 (3.72)
3:1	No	0.90	6.22	62.22	3.48 (3.29)
2:1	50 °C	0.90	7.21	63.09	4.09 (3.97)
2:1	70 °C	0.90	7.88	63.66	4.51 (4.43)
2:1	90 °C	0.88	6.47	64.74	4.34 (4.20)

^a Thermal annealing for 10 min. ^b Average value from ten devices.

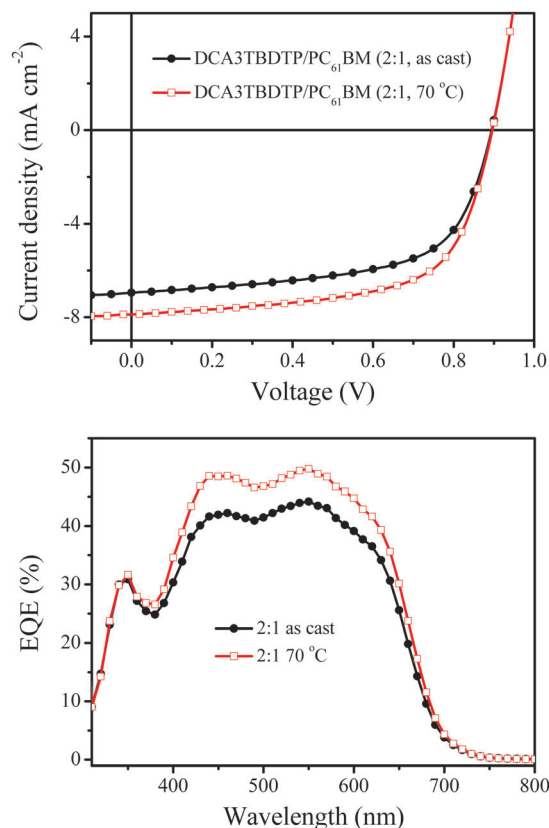


Fig. 5 (a) J - V characteristics and (b) EQE curves of the devices based on DCA3TBDTP/PC₆₁BM (2:1, w/w) before and after thermal annealing at 70 °C.

morphology of the active layer. Therefore, thermal annealing in the range of 50–90 °C was also employed to further optimize the device performance. With increasing the annealing temperature, the values of J_{sc} and FF increased significantly compared to the pristine ones. Interestingly, the V_{oc} of the BHJ solar cells remained almost constant before and after thermal annealing, as high as ~ 0.90 V, which is similar with that of other reported BDT-based SMOSCs and is believed to be related to the deep HOMO (-5.25 eV) energy level of the molecule, DCA3TBDTP (Fig. 3b).^{6,11,23} The current density *versus* voltage (J - V) curves of the optimized devices before and after thermal annealing at 70 °C are shown in Fig. 5a. Finally, a PCE of 4.51% for the DCA3TBDTP-based small molecule OSC was obtained with a V_{oc} of 0.90 V, a J_{sc} of 7.88 mA cm^{-2} and a FF of 63.66%, when the device was fabricated with a donor-acceptor weight ratio of 2:1 after thermal annealing at 70 °C.

To further understand the photo-to-electron conversion efficiencies of the DCA3TBDTP-based solar cells in the UV-vis region, the EQE curves of the optimized BHJ devices based on DCA3TBDTP/PC₆₁BM (w:w, 2:1) are presented in Fig. 5b. The EQE curves show a broad response covering 300–700 nm, consistent with the absorption spectrum. It is worth pointing out that thermal annealing improved the photo-response of the active layer over the whole range, leading to an increased J_{sc} . The J_{sc} values (6.92 mA cm^{-2} and 7.86 mA cm^{-2}) were calculated from integration of the EQE curves, which were consistent with

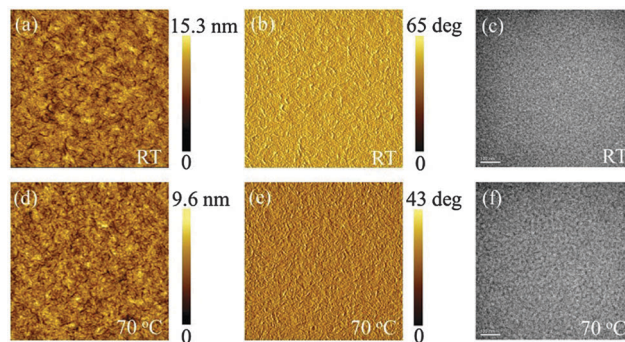


Fig. 6 Tapping-mode AFM height (a, d) and phase (b, e) images ($4 \mu\text{m} \times 4 \mu\text{m}$) and TEM images (c, f) of DCA3TBDTP/PC₆₁BM (2:1, w/w) blend films before and after thermal annealing at 70 °C. Scale bar: 100 nm.

the J_{sc} values (6.95 mA cm^{-2} and 7.88 mA cm^{-2}) obtained from the J - V measurements before and after thermal annealing at 70 °C for the DCA3TBDTP/PC₆₁BM (w:w, 2:1) devices.

Morphology and structural (X-ray) characterization

Atomic force microscopy (AFM) and transmission electron microscopy (TEM) were utilized to study the morphologies and phase separations of the DCA3TBDTP/PC₆₁BM (w:w, 2:1) blend films before and after thermal annealing at 70 °C. The active layer was spin-coated from a CHCl₃ solution on a glass/ITO/PEDOT:PSS substrate for the AFM measurements. The corresponding topography and phase images are shown in Fig. 6 (a, b – pristine films and d, e – thermal annealing films). Both blend films before and after thermal annealing exhibited a uniform and smooth surface, ensuring a better contact with the Ca/Al electrode and being beneficial for the increase in the charge collection efficiency. The root mean square (RMS) roughness is *ca.* 1.48 nm and 1.04 nm for the pristine film and thermally annealed blend film, respectively. The decreased RMS suggested that the quality of the DCA3TBDTP/PC₆₁BM blend film could be improved by thermal annealing. As shown in the TEM images (Fig. 6c and f), the thermally annealed blend film exhibits a better interpenetrating network containing a slightly larger nanoscale phase separation in the active layer. After annealing at 70 °C, the domain boundary intensity obviously reduced, which would decrease the trap state density existing in the boundary. Therefore, the transport and collection of the carrier charge was improved and the recombination current was also reduced. This is probably an important reason for the enhancement of J_{sc} and FF after thermal annealing in this work.^{23,30–33}

To further understand the relationship between the photovoltaic performance and the annealing temperature, the crystallinity of the DCA3TBDTP/PC₆₁BM blend film before and after thermal annealing at 70 °C was investigated using X-ray diffraction (XRD). As shown in Fig. 7, the first-order diffraction peak at $2\theta = 3.97^\circ$ corresponding to the (100) lattice plane of DCA3TBDTP with a d_{100} -spacing value of 22.2 \AA and the second-order diffraction peak (200) at $2\theta = 7.94^\circ$ were also clearly observed. The d_{100} -spacing is the distance between the main conjugated chains of the small molecules, separated by their side chains. The high intensity (100) diffraction peaks are due to the

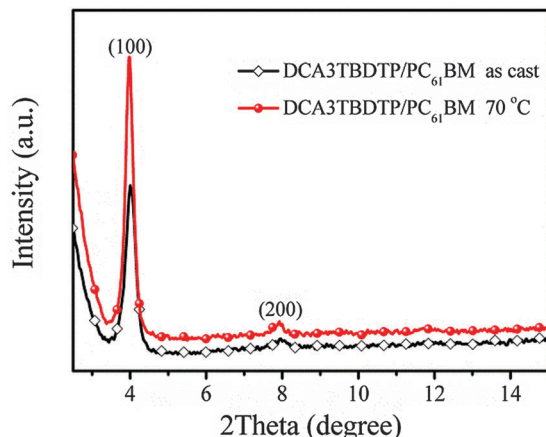


Fig. 7 XRD patterns of the DCA3TBDTP/PC₆₁BM films spin-coated from a CHCl₃ solution before and after thermal annealing at 70 °C.

presence of many alkyl side chains around the main chain, which were featured by the solution-processed small molecules as reported.^{1,18} Therefore the presence of these diffraction peaks indicated that the blend film exhibited an obvious ordered arrangement before and after thermal annealing. However, compared with the pristine film, the intensity of the diffraction peak of the annealed film was significantly enhanced and the half-band width was also narrowed, indicating that the ordered arrangement and degree of crystallinity was further improved in the active layer after thermal annealing.^{23,32} This is also in good agreement with the DSC results formerly discussed. The enhanced crystallinity associated with the stronger π - π stacking ability after thermal annealing could improve the carrier mobility which is beneficial to the carrier transport and collection, resulting in an improved J_{sc} and FF.^{31,32,34}

Hole mobility

The hole mobility of the DCA3TBDTP/PC₆₁BM blend film before and after thermal annealing at 70 °C was explored by the space-charge-limited current (SCLC) model³⁵ using a device configuration of ITO/PEDOT:PSS/DCA3TBDTP:PC₆₁BM (2:1, 100 nm)/Au (Fig. 8). The calculated hole mobility values of the blend films were $1.34 \times 10^{-4} \text{ cm}^2 (\text{V s})^{-1}$ and $2.74 \times 10^{-4} \text{ cm}^2 (\text{V s})^{-1}$ before and after thermal annealing, respectively. The results indicated that thermal annealing contributes to the improvement of the hole mobility, which was another important factor for the enhanced device performance after thermal annealing at a relatively low temperature.

Conclusion

A new small molecule DCA3TBDTP based on alkoxyphenyl substituted benzo[1,2-*b*:4,5-*b'*]dithiophene, terthiophene and octyl cyanoacetate was designed and synthesized by Stille coupling and Knoevenagel reactions. The small molecule exhibited good thermal stability, solubility and a deep HOMO energy level. As a weak electron donor, the alkoxyphenyl group as a conjugated side chain was introduced into the molecular backbone without having an obvious influence on the optical band gap and

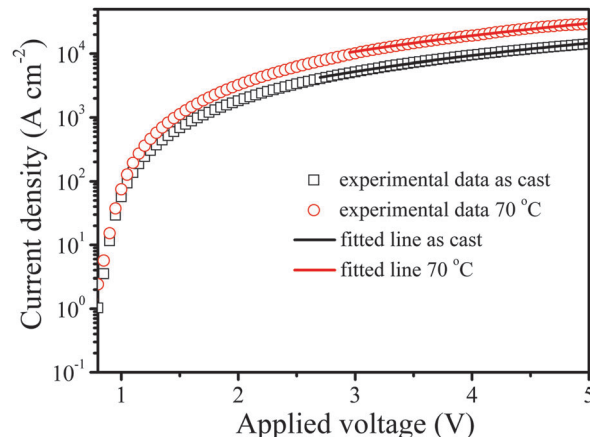


Fig. 8 Current density (J)-voltage (V) curves for DCA3TBDTP based devices (the symbols are experimental data for hole transport, and the lines are fitted according to the space-charge-limited-current model).

crystallinity. Solution-processed organic solar cells based on DCA3TBDTP and PC₆₁BM exhibited a PCE of 4.51% with a high V_{oc} of 0.90 V after thermal annealing at only 70 °C. The encouraging results reveal that the alkoxyphenyl substituted benzo[1,2-*b*:4,5-*b'*]dithiophene derivative is a prospective two-dimensional heterocyclic core in constructing donor-acceptor type small molecules for high-efficiency solution-processed organic solar cells.

Acknowledgements

This work was supported by the National Natural Science Foundation of China (21204097, 21274134, 51173199, 51303197 and 61405209), the Ministry of Science and Technology of China (2014CB643501, 2010DFA52310), the Danish National Research Foundation, and Qingdao Municipal Science and Technology Program (11-2-4-22-hz and 14-2-4-28-jch). The work was carried out in the Danish Chinese Centre of Organic based Photovoltaics with Morphological Control. Support from the Sino-Danish Centre for Education and Research (SDC) is also fully acknowledged.

Notes and references

- 1 Y. S. Liu, X. J. Wan, F. Wang, J. Y. Zhou, G. K. Long, J. G. Tian and Y. S. Chen, *Adv. Mater.*, 2011, **23**, 5387.
- 2 S. C. Price, A. C. Stuart, L. Q. Yang, H. X. Zhou and W. You, *J. Am. Chem. Soc.*, 2011, **133**, 4625.
- 3 H. Y. Chen, J. H. Hou, S. Q. Zhang, Y. Y. Liang, G. W. Yang, Y. Yang, L. P. Yu, Y. Wu and G. Li, *Nat. Photonics*, 2009, **3**, 649.
- 4 Y. Y. Liang and L. P. Yu, *Acc. Chem. Res.*, 2010, **43**, 1227.
- 5 L. J. Huo, J. H. Hou, S. Q. Zhang, H. Y. Chen and Y. Yang, *Angew. Chem., Int. Ed.*, 2010, **49**, 1500.
- 6 B. Kan, Q. Zhang, M. M. Li, X. J. Wan, W. Ni, G. K. Long, Y. C. Wang, X. Yang, H. R. Feng and Y. S. Chen, *J. Am. Chem. Soc.*, 2014, **136**, 15529.
- 7 Z. C. He, C. M. Zhong, S. J. Su, M. Xu, H. B. Wu and Y. Cao, *Nat. Photonics*, 2012, **6**, 591.

- 8 Y. H. Liu, J. B. Zhao, Z. K. Li, C. Mu, W. Ma, H. W. Hu, K. Jiang, H. R. Lin, H. Ade and H. Yan, *Nat. Commun.*, 2014, **5**, 5293.
- 9 Y. S. Chen, X. J. Wan and G. Long, *Acc. Chem. Res.*, 2013, **46**, 2645.
- 10 Y. Z. Lin, Y. F. Li and X. W. Zhan, *Chem. Soc. Rev.*, 2012, **41**, 4245.
- 11 J. Y. Zhou, X. J. Wan, Y. S. Liu, Y. Zuo, Z. Li, G. K. He, G. K. Long, W. Ni, C. X. Li, X. C. Su and Y. S. Chen, *J. Am. Chem. Soc.*, 2012, **134**, 16345.
- 12 S. L. Shen, P. Jiang, C. He, J. Zhang, P. Shen, Y. Zhang, Y. P. Yi, Z. J. Zhang, Z. B. Li and Y. F. Li, *Chem. Mater.*, 2013, **25**, 2274.
- 13 Y. Z. Lin, L. C. Ma, Y. F. Li, Y. Q. Liu, D. B. Zhu and X. W. Zhan, *Adv. Energy Mater.*, 2013, **3**, 1166.
- 14 D. Deng, Y. J. Zhang, L. Yuan, C. He, K. Lu and Z. X. Wei, *Adv. Energy Mater.*, 2014, **4**, 1400538.
- 15 W. Ni, X. J. Wan, M. M. Li, Y. C. Wang and Y. S. Chen, *Chem. Commun.*, 2015, **51**, 4936.
- 16 N. Lim, N. Cho, S. Paek, C. Kim and J. K. Lee, *Chem. Mater.*, 2014, **26**, 2283.
- 17 Y. J. Kim, J. Y. Baek, J. J. Ha, D. S. Chung, S. K. Kwon, C. E. Park and Y. H. Kim, *J. Mater. Chem. C*, 2014, **2**, 4937.
- 18 J. Y. Zhou, Y. Zuo, X. J. Wan, G. K. Long, Q. Zhang, W. Ni, Y. S. Liu, Z. Li, G. K. He, C. X. Li, B. Kan, M. M. Li and Y. S. Chen, *J. Am. Chem. Soc.*, 2013, **135**, 8484.
- 19 W. Ni, M. M. Li, X. J. Wan, H. R. Feng, B. Kan, Y. Zuo and Y. S. Chen, *RSC Adv.*, 2014, **4**, 31977.
- 20 J. Yuan, L. Xiao, B. Liu, Y. F. Li, Y. H. He, C. Y. Pan and Y. P. Zou, *J. Mater. Chem. A*, 2013, **1**, 10639.
- 21 W. C. Chen, Z. K. Du, L. L. Han, M. J. Xiao, W. F. Shen, T. Wang, Y. H. Zhou and R. Q. Yang, *J. Mater. Chem. A*, 2015, **3**, 3130.
- 22 Z. K. Du, W. C. Chen, S. G. Wen, S. L. Qiao, Q. Liu, D. Ouyang, N. Wang, X. C. Bao and R. Q. Yang, *ChemSusChem*, 2014, **7**, 3319.
- 23 Z. K. Du, W. C. Chen, Y. H. Chen, S. L. Qiao, X. C. Bao, S. G. Wen, M. L. Sun, L. L. Han and R. Q. Yang, *J. Mater. Chem. A*, 2014, **2**, 15904.
- 24 Q. C. Yu, W. F. Fu, J. H. Wan, X. F. Wu, M. M. Shi and H. Z. Chen, *ACS Appl. Mater. Interfaces*, 2014, **6**, 5798.
- 25 J. H. Huang, X. Wang, X. Zhang, Z. X. Niu, Z. H. Lu, B. Jiang, Y. X. Sun, C. L. Zhan and J. N. Yao, *ACS Appl. Mater. Interfaces*, 2014, **6**, 3853.
- 26 M. J. Frisch, G. W. Trucks, H. B. Schlegel, G. E. Scuseria, M. A. Robb, J. R. Cheeseman, G. Scalmani, V. Barone, B. Mennucci, G. A. Petersson, H. Nakatsuji, M. Caricato, X. Li, H. P. Hratchian, A. F. Izmaylov, J. Bloino, G. Zheng, J. L. Sonnenberg, M. Hada, M. Ehara, K. Toyota, R. Fukuda, J. Hasegawa, M. Ishida, T. Nakajima, Y. Honda, O. Kitao, H. Nakai, T. Vreven, J. A. Montgomery, J. E. Peralta Jr., F. Ogliaro, M. Bearpark, J. J. Heyd, E. Brothers, K. N. Kudin, V. N. Staroverov, T. Keith, R. Kobayashi, J. Normand, K. Raghavachari, A. Rendell, J. C. Burant, S. S. Iyengar, J. Tomasi, M. Cossi, N. Rega, J. M. Millam, M. Klene, J. E. Knox, J. B. Cross, V. Bakken, C. Adamo, J. Jaramillo, R. Gomperts, R. E. Stratmann, O. Yazyev, A. J. Austin, R. Cammi, C. Pomelli, J. W. Ochterski, R. L. Martin, K. Morokuma, V. G. Zakrzewski, G. A. Voth, P. Salvador, J. J. Dannenberg, S. Dapprich, A. D. Daniels, O. Farkas, J. B. Foresman, J. V. Ortiz, J. Cioslowski and D. J. Fox, *Gaussian 09, revision b.01*, Gaussian, Inc., Wallingford, CT, 2010.
- 27 C. T. Lee, W. T. Yang and R. G. Parr, *Phys. Rev. B: Condens. Matter Mater. Phys.*, 1988, **37**, 785.
- 28 A. D. Becke, *J. Chem. Phys.*, 1993, **98**, 5648.
- 29 W. J. Hehre, R. Ditchfield and J. A. Pople, *J. Chem. Phys.*, 1972, **56**, 2257.
- 30 H. Y. Wang, F. Liu, L. J. Bu, J. Gao, C. Wang, W. Wei and T. P. Russell, *Adv. Mater.*, 2013, **25**, 6519.
- 31 W. L. Leong, G. C. Welch, J. Seifter, J. H. Seo, G. C. Bazan and A. J. Heeger, *Adv. Energy Mater.*, 2013, **3**, 356.
- 32 L. M. Chen, Z. R. Hong, G. Li and Y. Yang, *Adv. Mater.*, 2009, **21**, 1434.
- 33 G. D. Wei, S. Y. Wang, K. Sun, M. E. Thompson and S. R. Forrest, *Adv. Energy Mater.*, 2011, **1**, 184.
- 34 J. Liu, H. Choi, J. Y. Kim, C. Bailey, M. Durstock and L. M. Dai, *Adv. Mater.*, 2012, **24**, 538.
- 35 V. D. Mihailetschi, J. Wildeman and P. W. M. Blom, *Phys. Rev. Lett.*, 2005, **94**, 126602.